

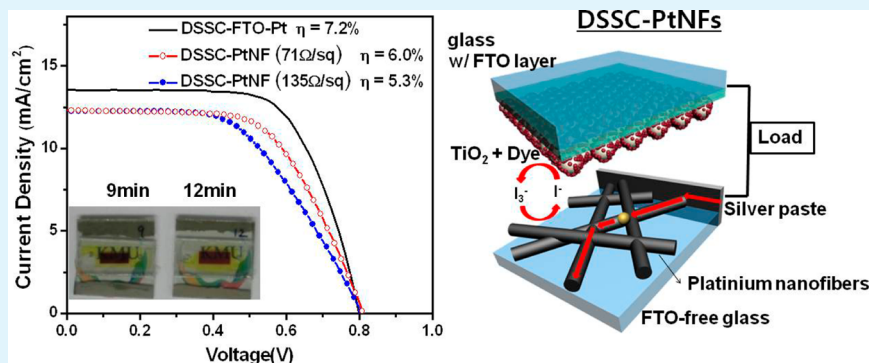
# Catalytic, Conductive, and Transparent Platinum Nanofiber Webs for FTO-Free Dye-Sensitized Solar Cells

Jongwook Kim,<sup>†,‡</sup> Jonghyun Kang,<sup>§</sup> Uiyoung Jeong,<sup>§</sup> Heesuk Kim,<sup>†</sup> and Hyunjung Lee<sup>\*,§</sup>

<sup>†</sup>Hybrid Polymer Materials Research Center, Korea Institute of Science and Technology, 39-1 Hawolgok-dong Seongbuk-gu Seoul, 130-650, Republic of Korea

<sup>§</sup>School of Advanced Materials Engineering, Kookmin University, 861-1 Jeongneung-Dong, Seoul, 136-702, Republic of Korea

## Supporting Information



**ABSTRACT:** We report a multifunctional platinum nanofiber (PtNF) web that can act as a catalyst layer in dye-sensitized solar cell (DSSC) to simultaneously function as a transparent counter electrode (CE), i.e., without the presence of an indium-doped tin oxide (ITO) or fluorine-doped tin oxide (FTO) glass. This PtNF web can be easily produced by electrospinning, which is highly cost-effective and suitable for large-area industrial-scale production. Electrospun PtNFs are straight and have a length of a few micrometers, with a common diameter of 40–70 nm. Each nanofiber is composed of compact, crystalline Pt grains and they are well-fused and highly interconnected, which should be helpful to provide an efficient conductive network for free electron transport and a large surface area for electrocatalytic behavior. A PtNF web is served as a counter electrode in DSSC and the photovoltaic performance increases up to a power efficiency of 6.0%. It reaches up to 83% of that in a conventional DSSC using a Pt-coated FTO glass as a counter electrode. Newly designed DSSCs containing PtNF webs display highly stable photoelectric conversion efficiencies, and excellent catalytic, conductive, and transparent properties, as well as long-term stability. Also, while the DSSC function is retained, the fabrication cost is reduced by eliminating the transparent conducting layer on the counter electrode. The presented method of fabricating DSSCs based on a PtNF web can be extended to other electrocatalytic optoelectronic devices that combine superior catalytic activity with high conductivity and transparency.

**KEYWORDS:** platinum, nanofiber, FTO-free, dye-sensitized solar cells, long-term stability, catalytic transparent electrodes

## 1. INTRODUCTION

Dye-sensitized solar cells (DSSC) have been recognized as a substitute for silicon-based solar cells because of their inherently low material costs.<sup>1,2</sup> Unfortunately, they require two transparent conductive oxide (TCO) electrodes constructed of indium-doped tin oxide (ITO) or fluorine-doped tin oxide (FTO) within a multilayered structure. It is this structural requirement that forms the major obstacle for reducing the overall fabrication costs of DSSCs. As a result, research is focused on the search for new materials and processes that can economize/simplify the current multilayer system, and at the same time, maintain superior photoelectric performance.<sup>3,4</sup> With respect to the transparent electrodes, there have been efforts to replace TCO by carbon nanotubes,<sup>5,6</sup> graphenes,<sup>7,8</sup> and metal nanowires,<sup>9–14</sup> because of their low production costs and flexibility. Electrodes made of such structures are often

tested in different types of photovoltaic cells, which sometimes show similar performance as the typical TCO electrode.<sup>9,11,15</sup> However, although most studies have confirmed that these materials can indeed replace TCO, they do not really address the structural innovation of the photovoltaic cells. Moreover, the materials involved are still of limited use, because of factors such as low long-term stability and poor large-area processability. In this study, we developed a multifunctional Pt nanofiber (PtNF) web that can act as a catalyst layer in DSSC to simultaneously function as a transparent counter electrode (CE), i.e., without the presence of an additional TCO layer. This PtNF web can be easily produced by electrospinning,<sup>16,17</sup>

Received: January 15, 2013

Accepted: March 21, 2013

Published: March 21, 2013

which is highly cost-effective and suitable for large-area industrial-scale production. Newly designed DSSCs containing PtNF webs display highly stable photoelectric conversion efficiencies, and excellent catalytic, conductive, and transparent properties, as well as long-term stability.

The typical DSSC structure contains two TCO layers, which function either as the photoelectrode or the CE (Figure 1a).

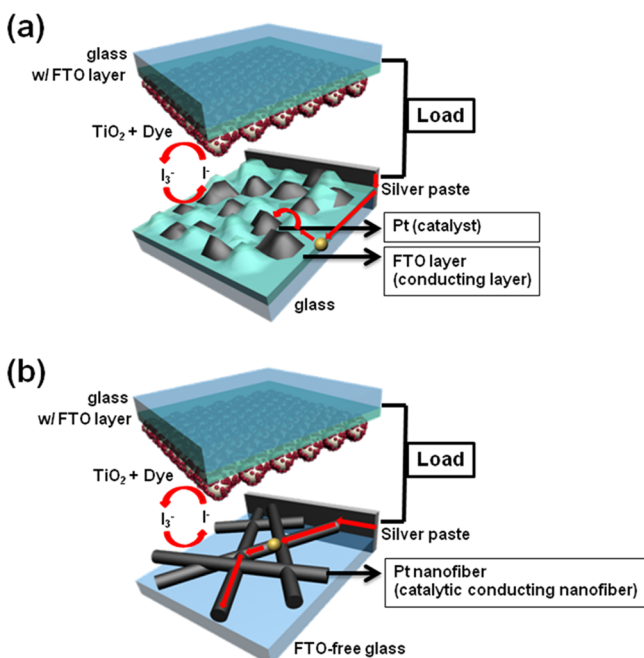


**Figure 1.** Schematic representation of DSSCs fabricated (a) with Pt nanofiber networks as counter electrodes (DSSC-PtNF) or (b) with a Pt-spun-coated FTO counter electrode (DSSC-FTO-Pt).

The photoelectrode should combine optical transparency for the collection of sunlight with electrical conductivity for the transport of electrons. The CE plays a key role in that it should act as an electrocatalyst that aids in the reduction of the iodide electrolyte. Thus, typical CEs are prepared with an additional Pt coating on the TCO layer. In order to decrease the amount of material and the processing costs, these CEs should ideally be replaced by a single layer that is both catalytic and transparent. For this reason, a catalytic carbon black film has replaced the Pt-coated TCO layer as the CE even though it is not transparent at all.<sup>18</sup> Recently, electrocatalytic transparent CNT films were reported, and these have replaced the TCO layer as well as the Pt catalyst in DSSCs.<sup>19,20</sup> However, they suffer from low sheet conductance and light transmittance. Highly conductive polymer films have also shown promise in TCO- and Pt-less counter electrodes although so far, a crucial limitation has been their low air stability.<sup>21</sup>

Figure 1b demonstrates schematically how we have modified the morphology of the Pt catalyst on the CE in DSSCs without the TCO layer. Instead of spin-coating Pt on the roughened TCO surface, a percolated PtNF web was fabricated on a bare glass substrate by electrospinning.<sup>16,17</sup> As Pt is a conductive metal as well as a good catalyst, such a percolated web structure enables efficient electron transport to the sites where the electrocatalytic reaction occurs. In addition, the electron transport step from TCO to Pt is absent; this enhances the cell's operational stability, which may otherwise be affected by the degradation of either the TCO layer or the contact between

Pt and TCO. Pt layers in DSSCs operate, even under harsh conditions, over long periods of time both as a catalyst and as a transparent electrode.<sup>22</sup> It has been reported that similarly structured metal nanofiber webs composed of silver or copper exhibited superior conductivity and transparency,<sup>9–13</sup> although they do not show catalytic behavior in DSSC. Moreover, reports state that the performance of these silver- or copper-based devices can be readily degraded. Carbonaceous materials are considered as alternatives, but in spite of their conductive and catalytic properties, they are limited in their optical transparency. At this point, it can therefore be said that the PtNF web is a unique material that unifies the transparent electrode layer and the catalyst layer into one film of exceptional long-term stability, which will be discussed in more detail below.

## 2. EXPERIMENTAL SECTION

**2.1. Fabrication of the Pt Nanofiber Web.** Our method for the fabrication of PtNF is essentially based on methods reported previously.<sup>16,17</sup> A viscous solution of polyvinylpyrrolidone (PVP) and the Pt precursor dihydrogen-hexachloroplatinate(IV)-hexahydrate ( $\text{H}_2\text{PtCl}_6 \cdot 6\text{H}_2\text{O}$ ) was electrospun on glass substrates in the form of NFs, and then, thermally annealed at 450 °C.<sup>17</sup> The concentration of PVP and Pt precursor as well as the solvent mixture ratio were varied to optimize the electrospinning behavior and to control the diameter of the nanofibers. A concentration of 0.1 g/mL-PVP (MW = 1 300 000) and 0.25 g/mL  $\text{H}_2\text{PtCl}_6 \cdot 6\text{H}_2\text{O}$  in a 1:1:2 water/ethanol/DMF mixture was found to give rise to the lowest sheet resistance with maximum transmittance of the fabricated PtNF webs. Electrospinning was conducted at a voltage between the 22 gauge needle and an earthed metal plate of 1 kV/cm, at a solution injection speed of 0.8  $\mu\text{L}/\text{min}$ . To obtain a uniform distribution of nanofibers over the entire surface area, glass substrates were fixed on a horizontally moving plate. The density of nanofibers per area could be readily controlled by varying the electrospinning time. As such, a uniform Pt NF film of any size and density could be fabricated.

**2.2. DSSC Fabrication.** A thin compact layer of  $\text{TiO}_2$  (ca. 40 nm) was coated onto FTO glass by spin coating a Ti(IV)bis-(ethylacetato)-diisopropoxide solution (sol-gel hydrolysis) and calcination at 450 °C, by preventing the direct contact of the electrolytes with the FTO glass. A  $\text{TiO}_2$  nanoparticle layer was prepared on the FTO substrate by doctor blading a paste of  $\text{TiO}_2$  nanoparticles (ca. 20 nm, DSL 18NR-T, Dyesol) with a thickness of a single scotch tape layer (ca. 30  $\mu\text{m}$ ). The  $\text{TiO}_2$  film was then calcined in air at 500 °C for two hours at a low heating rate (0.2 °C/min) to remove the organic components, leaving behind air cavities in the titania matrix. The thickness of the  $\text{TiO}_2$  film used in this work was controlled at 12 mm over a 20 mm  $\times$  20 mm area. The  $\text{TiO}_2$  films were immersed for 1 day in an ethanol solution containing 0.5 mM of purified N719 dye, after which the dye-adsorbed  $\text{TiO}_2$  electrodes were rinsed with ethanol and dried. A counter electrode was prepared by electrospinning a  $\text{H}_2\text{PtCl}_6$  solution onto the glass substrate as described above. A uniform PtNF webs on a glass substrate was served as a counter electrode. The dye-adsorbed electrode and the counter electrode were assembled using a 25-mm-thick Surlyn sheet (DuPont 1702) as a spacer. The liquid electrolytes consisted of 0.7 M 1-butyl-3-methylimidazolium iodide, 0.03 M iodine ( $\text{I}_2$ ), 0.1 M guanidium thiocyanate, and 0.5 M 4-tert-butylpyridine in a mixture of ACN and valeronitrile (85:15 v/v).

**2.3. Characterization.** The morphology of electrospun nanofibers was investigated using a field-emission scanning electron microscope (FE-SEM, JSM-6701F, JEOL) and high resolution-transmittance electron microscopy (HR-TEM, Tecnai G2, FEI Hong Kong Co. Ltd.). AFM images were recorded at room temperature on a commercial AFM (Asylum Research MFP3D) in noncontact mode (AC mode) with 10 nm standard cantilevers (AC160TS, Olympus). Conductive atomic force microscopy imaging was performed by the use of an ORCA module (Asylum Research MFP-3D) in noncontact

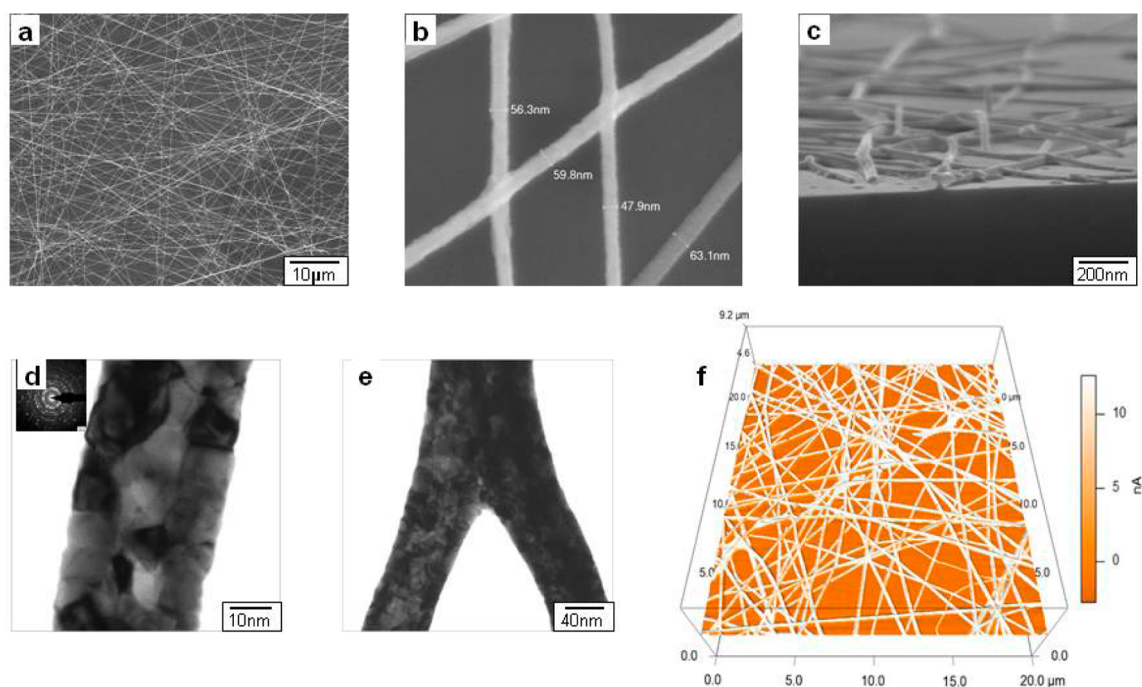


**Figure 2.** (a) Scanning electron microscopy (SEM) images of Pt nanofiber networks with varying densities of nanofibers per unit area with 81% transmittance (%T) and  $106 \Omega/\text{sq}$  sheet resistance. (b) Zoomed-in image of the interconnected nanofibers. (c) Tilted cross-section image. (d, e) Transmission electron microscopy (TEM) image of the Pt nanofibers. The electron diffraction pattern (d, inset) indicates that the grains composing the nanofiber are well crystallized, while the EDS spectrum shows only peaks indicative of Pt, except for the carbon and copper signals of TEM grid. (f) Conductive mode-atomic force microscopy image of the Pt nanofibers. Topography is three-dimensionally displayed and current is displayed in color.

mode with a doped silicon tip (Electri-Lever, AC240TM, Olympus). The sample bias was applied to the silver electrode coated on the PtNFs film via a wire from the ORCA holder. Photocurrent–voltage measurements were performed using a Keithley model 2400 source measuring unit. A 1000 W xenon lamp (Spectra-Physics) served as the light source and its light intensity was adjusted using a NREL-calibrated Si solar cell equipped with a KG-5 filter for approximating AM 1.5G one-sun light intensity. Impedance measurements were performed under the same conditions, at frequencies between 0.1–500 kHz with an ac signal of 10 mV amplitude using an iviumstat electrochemical interface (Ivium technologies). The applied bias voltage and ac amplitude were set at the  $V_{oc}$  level of the DSSC. Transport and recombination properties were measured under  $100 \text{ mW}/\text{cm}^2$  illumination by IMPS and IMVS using the same equipment as used for the impedance measurements.

### 3. RESULTS AND DISCUSSION

**3.1. Electrical and Optical Properties of Electrospun Pt Nanofibers.** The PtNF web is fabricated in two steps: electrospinning of the PVP nanofibers containing the ionic Pt precursor  $\text{H}_2\text{PtCl}_6 \cdot 6\text{H}_2\text{O}$  and thermal annealing to decompose the PVP and reduce the precursor to pure metallic Pt. The SEM images in Figure 2a–c show the morphology of the as-fabricated PtNF web. Each nanofiber is straight and has a length of a few micrometers, with a common diameter of 40–70 nm (Figure 2b). The TEM image shows a concentric diffraction pattern (Figure 2d), indicating that each nanofiber is composed of compact, crystalline Pt grains without any remaining polymers, which should be helpful to obtain a high electric conductivity. Additionally, the nanofiber web is highly interconnected as is indicated clearly by the fused junction in Figure 2e. Such a well-fused PtNF web should function as an efficient conductive network for free electron transport, as demonstrated in Figure 1b. This is further evidenced by the

conductive-mode AFM measurements shown in Figure 2f, where the white color displays the current flow between the AFM tip and the PtNF web. We observed that the microscopic structure stretches over the whole surface of the macroscopic substrate because of the use of an automatic motion-controlled robot arm with an electrospinning unit. It should also be noted that there is no significant difference in the amount of the Pt precursor needed per unit surface area to fabricate PtNF webs ( $\sim 50 \mu\text{g}/\text{cm}^2$  for DSSC-PtNF #2 in Table 1) and for the

**Table 1.** Light Conversion Efficiency ( $\eta$ ) and Related Photovoltaic Parameters of the DSSCs

counter electrode	$R_s(\Omega/\text{sq})$	$V_{oc}(\text{V})$	$J_{sc}(\text{mA}/\text{cm}^2)$	FF (%)	$\eta$ (%)
PtNF #1	135	0.81	12.3	53.8	5.3
PtNF #2	71	0.81	12.3	60.4	6.0
FTO-Pt	11	0.80	13.5	66.4	7.2

coating of the Pt catalyst layer in conventional DSSCs ( $46 \mu\text{g}/\text{cm}^2$ ). Thus, considering that electrospinning is a standard technique, which is easily applicable to large-scale manufacturing,<sup>23</sup> the high cost of manufacturing TCO electrodes can be mitigated by producing DSSCs with PtNF web CEs.

The sheet resistance ( $R_s$ ) versus optical percent-transmittance data (%T at  $\lambda = 550 \text{ nm}$ ; by which the performance of a transparent electrode is assessed) of the PtNF web according to electrospinning time ( $t_{\text{spin}}$ ) is shown in Table S1 and Figure S1 in the Supporting Information. This shows the typical trend of decreasing  $R_s$  and %T with an increase in nanofiber density, which increases with  $t_{\text{spin}}$  (the SEM images of PtNF webs for different  $t_{\text{spin}}$  and %T spectra over a range of  $\lambda = 300\text{--}800 \text{ nm}$  are provided in Figures S2 and S3 in the

Supporting Information, respectively). In Figure 3, the sheet conductance ( $\sigma = 1/R_s$ ) is plotted as a function of  $t_{\text{spin}}$  and it

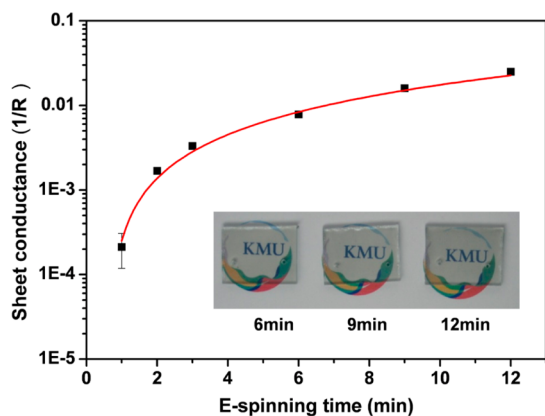


**Figure 3.** Plot of the measured sheet conductance ( $1/R_s$ ) of the PtNF networks as a function of electrospinning time ( $t$ ). The solid curve is a fit to percolation theory using the eq  $1/R_s \propto t^{1.33}$ . The photographs represent DSSCs with a PtNF web as the CE.

agrees well with the plot of the theoretical equation (eq 1) for two-dimensional rod percolation (solid line)<sup>24</sup>

$$\sigma \approx (N - N_C)^{1.33} \quad (1)$$

, where  $N$  is the density of conducting wires that is assumed to be directly proportional to  $t_{\text{spin}}$ . Here,  $N_C$  is the percolation threshold density, which is very small in the case of electrospun nanofibers that have extremely large aspect ratios of up to 100

000<sup>5</sup>. Our results show  $R_s$  of 128  $\Omega/\text{sq}$  at 81%T and 40  $\Omega/\text{sq}$  at 68%T, which is close to that of recently reported materials based on metal nanofibers, nanowire, or mesh structures. The  $R_s$  value of the PtNF web for a given %T is roughly six times higher than the highest values reported for similar structures composed of silver or copper.<sup>9–13</sup> This may be expected to be to the result of the intrinsic bulk conductivity of Pt ( $0.097 \times 10^6/(\text{cm } \Omega)$ ), which is approximately six times lower than that of silver and copper ( $0.596 \times 10^6/(\text{cm } \Omega)$  and  $0.63 \times 10^6/(\text{cm } \Omega)$ , respectively). Despite the somewhat higher  $R_s$ , it can be concluded that the use of the PtNF web particularly in DSSC is an indispensable choice with regard to catalytic behavior and long-term stability, as will be discussed below.

**3.2. Photovoltaic Performance of DSSCs Using Electrospun Pt Nanofibers.** DSSCs were fabricated by the standard procedure described in the Experimental Section. Reference cells with an FTO layer and Pt catalyst layer (DSSC-FTO-Pt) and test cells using the PtNF web (DSSC-PtNF) were prepared in an identical manner, except for their CE parts. Figure 4a shows the typical current voltage plots of these cells. The photovoltaic parameters, including the short-circuit photocurrent density ( $J_{\text{sc}}$ ), the open-circuit voltage ( $V_{\text{oc}}$ ), and the fill factor (FF) of these cells are indicated in Table 1. The overall photoelectric conversion efficiency ( $\eta$ ) was calculated using the equation  $\eta = J_{\text{sc}} V_{\text{oc}} \text{FF} / P$ , where  $P$  is the power density of the incident light ( $100 \text{ mW}/\text{cm}^2$ ). At  $\eta$  of the reference cell (DSSC-FTO-Pt) of 7.2%,  $\eta$  of our DSSC-PtNFs with  $R_s$  of either 71  $\Omega/\text{sq}$  ( $t_{\text{spin}} = 12 \text{ min}$ ) or 135  $\Omega/\text{sq}$  ( $t_{\text{spin}} = 9 \text{ min}$ ) were 6 and 5.3%, respectively. The enhancement of  $\eta$  at higher nanofiber density was attributed to the increased FF, whereas

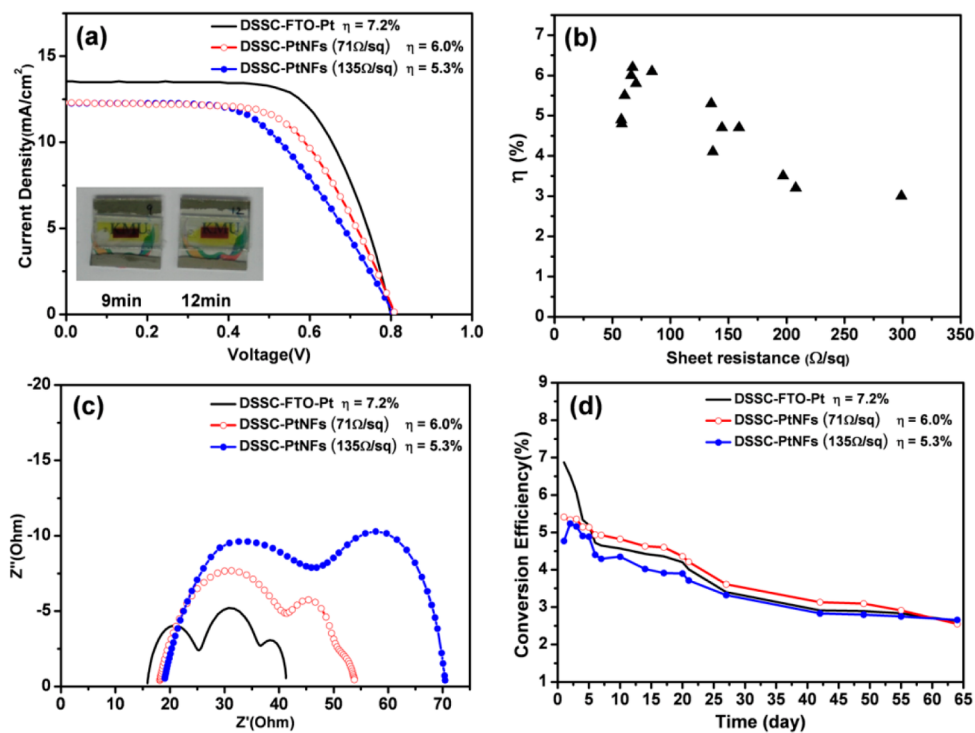


**Figure 4.** (a) Current–voltage curves of dye-sensitized solar cells (DSSCs) fabricated with Pt nanofiber networks as the counter electrodes (CEs) and sheet resistances of 71  $\Omega/\text{sq}$  (open circles) and 135  $\Omega/\text{sq}$  (closed circles). The black line indicates the reference cell with a standard FTO CE. The inset shows a photograph of the fabricated cell, where the upper glass slide is the FTO photoelectrode and the bottom slide is the PtNF CE, which is deposited on a glass slide that is thinner than the FTO glass. (b) Power conversion efficiencies ( $\eta$ ) of the Pt nanofiber-DSSCs with varying sheet resistances of the Pt nanofiber CEs. (c) Nyquist plots as obtained from electrochemical impedance measurements of DSSCs with different CEs in (a). (d) Device performance of DSSCs with different CEs stored at ambient conditions for a period of 65 days.

$V_{oc}$  and  $J_{sc}$  were unaffected. Indeed, FF was found to be related to the internal series resistance of the cells. The small surface area and high electrical resistance of the sparse PtNF web increased the series resistance, resulting in a low FF. The loss in optical transmittance of the dense PtNF web is compensated by its higher electrical conductivity and its enhanced catalytic behavior. Multiple other DSSC-PtNFs with varying nanofiber densities (and thus varying  $R_s$ ) were tested as well, where the plot of  $\eta$  vs  $R_s$  of these cells shows a trend of increasing  $\eta$  with decreasing  $R_s$  (Figure 4b).

**3.3. Electrical Impedance Analysis on DSSCs with Pt Nanofibers.** To investigate the series resistance and catalytic activity, electrochemical impedance spectroscopy (EIS) under illumination was conducted on the same cells (i.e., those mentioned in Figure 4a and Table 1). The DSSC contains three spatially separated interfaces, i.e., the photoelectrode/TiO<sub>2</sub> interface, the TiO<sub>2</sub>/dye/electrolyte interface, and the electrolyte/CE interface. The impedance at the electrolyte/CE interface corresponds to  $R_{CT}$ . Figure 4c shows the Nyquist plot of typical DSSC-FTO-Pt and DSSC-PtNFs in an open circuit under 1 sun illumination (the corresponding Bode plot is shown in Figure S4 in the Supporting Information). The semicircles at the highest regime are related to the electrolyte/CE, assigned to  $R_{CT}$ .  $R_s$  includes the ohmic series resistance in this electrochemical cell while  $R_s$  can be obtained from the real component ( $Z'$ ) values. Table S2 in the Supporting Information lists the results of the electrochemical impedance analysis, including the  $R_{CT}$  and  $R_s$  values of the DSSCs. The  $R_s$  values of the DSSC-PtNFs did not significantly deviate from that of the DSSC-FTO-Pt. Furthermore, these values are relatively independent of the nanofiber density, indicating that the PtNF web on the insulating glass substrate without FTO layer functions efficiently as a conducting layer. On the other hand, the  $R_{CT}$  value decreased with increasing nanofiber density, implying that a denser PtNF network displays a higher catalytic activity. The lower  $R_{CT}$  value of the DSSC-PtNF was  $\sim 25.8 \Omega \text{ cm}^2$  at  $t_{spin} = 12$  min, which is slightly larger than that of the standard DSSC-FTO-Pt ( $R_{CT} = 9.65 \Omega \text{ cm}^2$ ), indicating that the catalytic activity of the PtNF web is quite comparable to that of the Pt layer coated on the FTO layer. The low  $R_{CT}$  of the FTO-Pt counter electrode may be ascribed to the fact that the roughened surface of the conventional FTO glass provides a large surface area at the electrolyte/CE interface (see Figure S5 in the Supporting Information). Although prepared on a highly flat glass substrate, the PtNF CEs have a comparable surface area because of the overlaid nanofibers (Figure 2c). The  $R_{CT}$  value for our DSSC-PtNFs, which is around  $30 \Omega \text{ cm}^2$ , is much lower than that reported for DSSCs based on other high-performance TCO-less CEs that employ carbon nanotubes or PEDOT:PSS.<sup>19–21</sup> It is, therefore, believed that the percolated network structure of the electrospun PtNF web is responsible for the high electrochemical catalytic activity as well as the high conductivity for electron transport.

**3.4. Long-Term Stability.** A second crucial advantage of the PtNF web for potential application in DSSCs is its long-term stability. As Pt is inert and only assists in the catalytic reaction, the PtNF web CE in the DSSC should endure long-time operation under the harsh photochemical condition required for harvesting light. We measured the performance of DSSC-PtNFs repeatedly for over two months (Figure 4d), and we saw a slowly decreasing  $\eta$ , similar to the reference DSSC-FTO-Pt. Although  $\eta$  of the reference cell was somewhat higher initially, it rapidly decreased within 1 week to similar

levels as observed for DSSC-PtNFs, and subsequently, a similar decreasing trend was observed for all DSSCs.

## 4. CONCLUSION

In conclusion, the electrospun Pt nanofiber web functions both as an efficient electrocatalytic layer for the reduction of the iodide present in the electrolyte and as the transparent electrode in DSSCs. DSSCs containing the web show stable photoelectric conversion efficiencies comparable to that of conventional DSSCs. Thus, although the DSSC function is retained, the fabrication cost is reduced by eliminating the TCO layer on the counter electrode. The presented method of fabricating DSSCs based on a Pt nanofiber web can be extended to other electrocatalytic optoelectronic devices that combine superior catalytic activity with high conductivity and transparency.

## ■ ASSOCIATED CONTENT

### Supporting Information

The optical transmittance at 550 nm of Pt nanofibers-coated films as a function of their electrical sheet resistance; SEM images of Pt nanofibers on the glass substrate depending on the electrospinning time; transmittance spectra of the samples with different electro-spinning times; Bode plots of DSSCs with different counter electrodes from the electrochemical impedance measurement; SEM images of (a) bare FTO glass and (b) FTO glass after Pt coating in conventional DSSCs. A brief statement in nonsentence format; electrical and optical properties of Pt nanofibers-coated films as a function of an electrospinning time; electrochemical impedance analysis results of DSSC-PtNFs as a function of an electrospinning time. This material is available free of charge via the Internet at <http://pubs.acs.org/>.

## ■ AUTHOR INFORMATION

### Corresponding Author

\*E-mail: [hyunjung@kookmin.ac.kr](mailto:hyunjung@kookmin.ac.kr). Phone: 82-2-910-4662. Fax: 82-2-910-4320.

### Present Address

<sup>‡</sup>Laboratoire de Physique de la Matière Condensée-Ecole Polytechnique, Palaiseau, FR 91128.

### Author Contributions

The manuscript was written through contributions of all authors. All authors have given approval to the final version of the manuscript.

### Notes

The authors declare no competing financial interest.

## ■ ACKNOWLEDGMENTS

H. Lee acknowledges the financial support for this work given by the National Research Foundation of Korea Grant funded by the Korean Government (MEST) (NRF-2009-C1AAA001-2009-0093049, 2012R1A2A2A01014288, and NRF-2011-0014376). In addition, this work was supported by another grant from the National Research Foundation of Korea funded by the Korea government (MEST) (R11-2005-048-00000-0). The authors appreciate Mr. Taiwan Kim for performing AFM measurements and Mr. Jinwook Oh for performing EIS measurements.

## ■ REFERENCES

- (1) O'Regan, B.; Gratzel, M. *Nature* **1991**, *353*, 737–740.

- (2) Gratzel, M. *Inorg. Chem.* **2005**, *44*, 6841–6851.
- (3) Kumar, A.; Zhou, C. W. *ACS Nano* **2010**, *4*, 11–14.
- (4) Hecht, D. S.; Hu, L.; Irvin, G. *Adv. Mater.* **2010**, *23*, 1482–1513.
- (5) Hu, L.; Hecht, D. S.; Gruner, G. *Nano Lett.* **2004**, *4*, 2513–2517.
- (6) Robert, C. T.; Teresa, M. B.; Jeremy, D. B.; Andrew, J. F.; Bobby, T.; Lynn, M. G.; Michael, J. H.; Jeffrey, L. B. *Adv. Mater.* **2009**, *21*, 3210–3216.
- (7) Bae, S.; Kim, H.; Lee, Y.; Xu, X.; Park, J.-S.; Zheng, Y.; Balakrishnan, J.; Lei, T.; Ri Kim, H.; Song, Y. I.; Kim, Y.-J.; Kim, K. S.; Ozyilmaz, B.; Ahn, J.-H.; Hong, B. H.; Iijima, S. *Nat. Nano* **2010**, *5*, 574–578.
- (8) Li, X.; Zhu, Y.; Cai, W.; Borysiak, M.; Han, B.; Chen, D.; Piner, R. D.; Colombo, L.; Ruoff, R. S. *Nano Lett.* **2009**, *9*, 4359–4363.
- (9) Lee, J. Y.; Connor, S. T.; Cui, Y.; Peumans, P. *Nano Lett.* **2008**, *8*, 689–692.
- (10) Rathmell, A. R.; Bergin, S. M.; Hua, Y.-L.; Li, Z.-Y.; Wiley, B. J. *Adv. Mater.* **2010**, *22*, 3558–3563.
- (11) Wu, H.; Hu, L.; Rowell, M. W.; Kong, D.; Cha, J. J.; McDonough, J. R.; Zhu, J.; Yang, Y.; McGehee, M. D.; Cui, Y. *Nano Lett.* **2010**, *10*, 4242–4248.
- (12) Rathmell, A. R.; Wiley, B. J. *Adv. Mater.* **2011**, *23*, 4798–4803.
- (13) van de Groep, J.; Spinelli, P.; Polman, A. *Nano Lett.* **2012**, *12*, 3138–3144.
- (14) Kuang, P.; Park, J.-M.; Leung, W.; Mahadevapuram, R. C.; Nalwa, K. S.; Kim, T.-G.; Chaudhary, S.; Ho, K.-M.; Constant, K. *Adv. Mater.* **2011**, *23*, 2469–2473.
- (15) Han, J.; Kim, H.; Kim, D. Y.; Jo, S. M.; Jang, S.-Y. *ACS Nano* **2010**, *4*, 3503–3509.
- (16) Lee, H.; Choi, S. H.; Jo, S. M.; Kim, D. Y.; Kwak, S.; Cha, M. W.; Kim, I. D.; Jang, S. Y. *J. Phys. D: Appl. Phys.* **2009**, *42*, 125409.
- (17) Shui, J. L.; Li, J. C. M. *Nano Lett.* **2009**, *9*, 1307–1314.
- (18) Murakami, T. N.; Ito, S.; Wang, Q.; Nazeeruddin, M. K.; Bessho, T.; Cesar, I.; Liska, P.; Humphry-Baker, R.; Comte, P.; Pechy, P.; Gratzel, M. J. *Electrochem. Soc.* **2006**, *153*, A2255–A2261.
- (19) Trancik, J. E.; Barton, S. C.; Hone, J. *Nano Lett.* **2008**, *8*, 982–987.
- (20) Lee, W. J.; Ramasamy, E.; Lee, D. Y.; Song, J. S. *ACS Appl. Mater. Interfaces* **2009**, *1*, 1145–1149.
- (21) Lee, K. S.; Lee, H. K.; Wang, D. H.; Park, N.-G.; Lee, J. Y.; Park, O. O.; Park, J. H. *Chem. Commun.* **2010**, *46*, 4505–4507.
- (22) Liang, H.-W.; Cao, X.; Zhou, F.; Cui, C.-H.; Zhang, W.-J.; Yu, S.-H. *Adv. Mater.* **2011**, *23*, 1467–1471.
- (23) Thavasi, V.; Singh, G.; Ramakrishna, S. *Energy Environ. Sci.* **2008**, *1*, 205–221.
- (24) Stauffer, G. *Introduction to Percolation Theory*; Taylor & Francis: London, 1985.